Available online at www.sciencedirect.com
SCIENCE DIRECT
Journal of Solid State Chemistry 179 (2006) 1383–1393
JOURNAL OF SOLID STATE CHEMISTRY
www.elsevier.com/locate/jssc

Amorphous and nanocrystalline titanium nitride and carbonitride materials obtained by solution phase ammonolysis of $Ti(NMe_2)_4$

Andrew W. Jackson[a], Olga Shebanova[b,c], Andrew L. Hector[a,*], Paul F. McMillan[b,c,*]

[a]*School of Chemistry, University of Southampton, Highfield, Southampton SO17 1BJ, UK*
[b]*Department of Chemistry and Materials Chemistry Centre, University College London, 20 Gordon Street, London WC1H 0AJ, UK*
[c]*Davy-Faraday Research Laboratory, The Royal Institution of Great Britain, 21 Albemarle Street, London W1X 4BS, UK*

Received 18 October 2005; received in revised form 6 January 2006; accepted 28 January 2006
Available online 3 March 2006

Abstract

Solution phase reactions between tetrakisdimethylamidotitanium ($Ti(NMe_2)_4$) and ammonia yield precipitates with composition $TiC_{0.5}N_{1.1}H_{2.3}$. Thermogravimetric analysis (TGA) indicates that decomposition of these precursor materials proceeds in two steps to yield rocksalt-structured TiN or Ti(C,N), depending upon the gas atmosphere. Heating to above 700 °C in NH_3 yields nearly stoichiometric TiN. However, heating in N_2 atmosphere leads to isostructural carbonitrides, approximately $TiC_{0.2}N_{0.8}$ in composition. The particle sizes of these materials range between 4–12 nm. Heating to a temperature that corresponds to the intermediate plateau in the TGA curve (450 °C) results in a black powder that is X-ray amorphous and is electrically conducting. The bulk chemical composition of this material is found to be $TiC_{0.22}N_{1.01}H_{0.07}$, or $Ti_3(C_{0.17}N_{0.78}H_{0.05})_{3.96}$, close to $Ti_3(C,N)_4$. Previous workers have suggested that the intermediate compound was an amorphous form of Ti_3N_4. TEM investigation of the material indicates the presence of nanocrystalline regions <5 nm in dimension embedded in an amorphous matrix. Raman and IR reflectance data indicate some structural similarity with the rocksalt-structured TiN and Ti(C,N) phases, but with disorder and substantial vacancies or other defects. XAS indicates that the local structure of the amorphous solid is based on the rocksalt structure, but with a large proportion of vacancies on both the cation (Ti) and anion (C,N) sites. The first shell Ti coordination is approximately 4.5 and the second-shell coordination ~5.5 compared with expected values of 6 and 12, respectively, for the ideal rocksalt structure. The material is thus approximately 50% less dense than known $Ti_x(C,N)_y$ crystalline phases.

Keywords: Titanium nitride; Ti_3N_4; Amorphous; Nanocrystalline; X-ray absorption spectroscopy; TEM; Raman scattering

1. Introduction

Titanium nitrides and carbonitrides are in demand because of their desirable properties. Titanium nitride films continue to find new applications related to their high hardness (machine tools and protective coatings in high-wear environments), resistance to chemical diffusion (microelectronics), biocompatibility (surgical tools and implants), low coefficient of friction (suspension components), attractive golden appearance (used in jewellery) and solar control properties [1]. These films are often produced by chemical vapour deposition (CVD) using titanium dialkylamides and ammonia as precursors as initially described by Fix et al. [2]. The CVD process is suggested to proceed via transamination reactions resulting in the gas phase formation of $Ti_{1+x}(NH_2)_2(NMe_2)_{4x}$ cages [3]. The thermal decomposition of these cages leads to the formation of rocksalt-structured TiN; however, it has been proposed that an intermediate compound with composition Ti_3N_4 might exist [3]. The existence of such a material has never been conclusively demonstrated; however, a Ti_3N_4 phase has been predicted theoretically to be stable in the spinel structure [4]. By analogy with the newly discovered nitride spinels Si_3N_4/Ge_3N_4 [5] and the Th_3P_4-type Zr_3N_4/Hf_3N_4 [6], it is of potential interest as a narrow bandgap semiconductor and as a high-hardness material.

*Corresponding authors. Fax: +44 2380 594125.
E-mail addresses: a.l.hector@soton.ac.uk (A.L. Hector), p.f.mcmillan@ucl.ac.uk (P.F. McMillan).

0022-4596/$ - see front matter © 2006 Elsevier Inc. All rights reserved.
doi:10.1016/j.jssc.2006.01.067

The reactions between transition metal dialkylamides and ammonia in solution to produce bulk nitrides were investigated by Baxter et al. [7] and previously by Brown and Maya [8]. The reaction of $Ti(NMe_2)_4$ with ammonia was found to produce a precipitate of composition $TiC_{1.2}N_{1.2}H_4$ which yielded TiN powders on thermolysis in He at $>700\,^{\circ}C$ [7]. Thermogravimetric analysis (TGA) revealed a plateau in the weight loss curves between 400 and 600 °C that was attributed to a higher nitride phase. Chemical analysis of the X-ray amorphous material indicated a composition $TiN_{1.2}$ "with a trace of carbon", and the solid compound was suggested to be an amorphous variety of Ti_3N_4 [7]. In the present study, we have investigated the nature of this material using a combination of X-ray absorption spectroscopy (XAS) and extended X-ray absorption fine structure (EXAFS) analysis, transmission electron microscopy (TEM), and Raman and FTIR spectroscopy.

$Ti(C,N)_x$ materials synthesized in this study were nanocrystalline (nc), or contained crystalline nanoparticles embedded in an amorphous matrix. Composites based on hard, nc materials in an amorphous (a) matrix, such as nc-TiN/a-Si_3N_4 and nc-TiC/a-C:H (C:H is hydrogenated carbonaceous material), have been shown to form ultrahard materials (hardness values up to 100 GPa have been claimed for nc-TiN/a-Si_3N_4 compared with 33 GPa for TiN itself, and 92 GPa for diamond) by inhibiting dislocation movement and growth within the hard material [9]. Previous reports on the synthesis of nc TiN_x powders include reactions of TiH_2 with NH_4Cl [10], decomposition of $TiCl_4L_x$ complexes (L is an N- or O-donor ligand) in NH_3 [11] and solid-state reactions of $TiCl_3$ with Mg_3N_2 or Ca_3N_2 with a diluting agent to control the reaction temperature [12].

2. Experimental section

All reagents and products were handled under dry nitrogen conditions; tetrahydrofuran (thf) used as a solvent was distilled over sodium/benzophenone. $Ti(NMe_2)_4$ (99.999%) was obtained from Epichem, TiN (99%) from Aldrich, electronic grade (99.999%) NH_3 from Air Products and ULSI grade (99.9999%) N_2 from BOC. $Ti(NMe_2)_4$ (2 cm^3) was dissolved in thf (50 cm^3) and exposed to gaseous NH_3 until no further precipitation occurred. The brown precipitate was collected by filtration and dried in vacuo, its composition was found to be $TiC_{0.49}N_{1.10}H_{2.32}$ (combustion C, H, N microanalysis and Ti by oxidative TGA). The filtrate was colourless and left no residue on evaporation. The highly air-sensitive precipitate was then heated at various temperatures under ULSI-grade nitrogen (70 $cm^3 min^{-1}$) on the TGA (Mettler Toledo TGA851e-glove box mounted) or under anhydrous NH_3 (50 $cm^3\,min^{-1}$) in a tube furnace (transferred to heating tube in the glove box). Samples were not found to be appreciably air sensitive after heating but were handled under N_2 for most measurements (PXD, XAS, analysis, Raman, IR) anyway.

Powder X-ray diffraction (PXD) data were collected using a Siemens D5000 diffractometer with Cu-$K_{\alpha 1}$ radiation. Lattice parameters and crystallite size information were obtained using the GSAS [13] package and the Gaussian instrumental peak shape was determined by refining a quartz standard. TEM data were recorded using a JEOL 3010 microscope with an Oxford Inca 100 energy-dispersive X-ray (EDX) microanalysis probe, the accelerating voltage was 300 kV. Additional TEM images and diffraction data were obtained using a JEOL-100cX instrument. Transmission powder IR experiments were carried out on pressed CsI disks with a Perkin Elmer Spectrum One spectrometer. IR reflectance spectra were obtained from pressed powders using a Bruker IFSv-66 instrument. Combustion (C, H, N) microanalysis data were provided by Medac Ltd. Conductivity measurements were carried out with a standard multimeter on pressed disk samples.

Raman spectra were obtained using a home-built high-throughput system [14] based on Kaiser® SuperNotch® filters, an Acton® 300 spectrograph system and a liquid-N_2-cooled back-thinned Si CCD detector. Spectra were excited using the 514.5 nm line of an Ar^+ laser or 633 nm line of a He–Ne laser, focused onto the sample using a 50× long working distance Mitutoyo objective. Raman scattering was collected in a 180° geometry through the same lens. Care was taken to maintain the laser power at minimal values (~1 mW) to minimize sample heating. No surface oxidation was detected. TiO_2 (rutile or anatase) is a very strong Raman scatterer, compared with the metallic TiN_x samples: the formation of even minute amounts of oxide is immediately detected by the Raman technique. The spectra obtained here were collected in an N_2-filled chamber (a diamond anvil cell loaded cryogenically with N_2 and held at minimal pressure, P~1–3 GPa).

XAS were collected in transmission mode on station 7.1 of the SRS at Daresbury Laboratory with Si-111 monochromator. Samples were diluted with dry boron nitride, pressed into disks and encapsulated in 6 μm Kapton film to avoid air exposure. Background subtraction was carried out using PAXAS [15] and the EXAFS were fitted with Excurve [16].

3. Results and discussion

3.1. Compositional studies, IR, Raman, TEM and PXD results

Typical transmission IR spectra of the brown precipitate obtained by reacting $Ti(NMe_2)_4$ with NH_3 in thf solution are shown in Fig. 1. Small variations in the composition of the precipitate are known to occur as a function of reaction conditions [17]. The corresponding IR spectra were likewise somewhat variable even when the reaction conditions were kept constant; however, the principal features remain

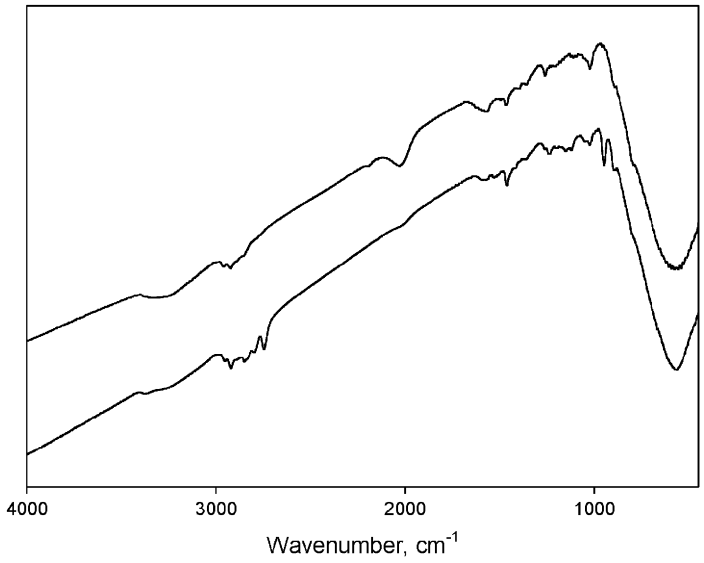

Fig. 1. Representative infrared spectra of precursor materials, showing variation in the composition immediately after precipitation.

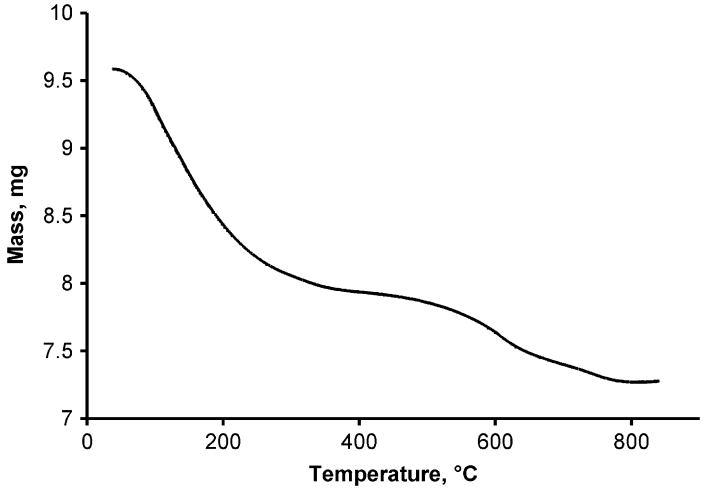

Fig. 2. TGA curve showing the two-stage thermal decomposition of precursor.

the same. The spectra are dominated by a strong M–N stretch at 560 cm^{-1}, with weaker ν(NH) (3250 cm^{-1}), ν(CH) (2920–2740 cm^{-1}) and δ(NH_2) (1590 cm^{-1}) bands (Fig. 1). This corresponds to a polymeric sol–gel-type material with bridging imide groups, some amide termini and some remaining dimethylamide groups. In some runs, a weak feature was observed near 2030 cm^{-1} which is tentatively assigned to Ti–H vibrations by analogy with the analogous Si/N system [18]. As found previously [7], the brown precipitate was found to decompose on heating in N_2 in two steps centred around 200 and 700 °C, respectively (Fig. 2).

To investigate the solid nitride phases which could be produced from the precipitate, annealing studies were carried out under high-purity N_2 and NH_3 atmospheres. Table 1 shows the chemical compositions and results of analysis of the PXD data obtained for the various materials. Compounds annealed to temperatures above the second step in the TGA curve in N_2 or NH_3 were crystalline with the rocksalt TiN or Ti(C,N) structure (Fig. 3). The refined lattice parameters were slightly larger than that of stoichiometric TiN, and they varied slightly as a function of the preparation conditions. This could be due to the presence of vacancies in the TiN structure, the substitution of C for N in some compounds, and the nc nature of the materials. Fitting of the PXD patterns for materials annealed between 850–1000 °C indicated average particle sizes of 8–12 nm (Table 1). This result was generally confirmed by TEM (Fig. 4). Examination of the sample annealed at 1000 °C in N_2 for 2 h showed a range of particles between 4.5–10.5 nm in dimension, with very few exceeding 10 nm. The samples annealed in nitrogen were always found to remain carbon rich, and the C content did not change as the annealing temperature was increased

Table 1
Composition and crystallographic data on products of annealing the precipitate

Sample preparation	Composition (%C, %H, %N)	PXD data
N_2, 450 °C for 2 h	4.04(2), 0.11(2), 21.80(5)	Amorphous
N_2, 1000 °C for 2 h	4.02(3), <0.1, 18.86(2)	$a = 4.2382(12)$ Å, 12 nm crystallite size
NH_3, 850 °C for 2 h	0.80(2), 0.20(2), 20.93(5)	$a = 4.2274(9)$ Å, 8 nm crystallite size
NH_3, 850 °C for 8 h	0.17(1), <0.1, 19.89(1)	$a = 4.2269(10)$ Å, 9 nm crystallite size
TiN standard	<0.1, <0.1, 21.36(6)	$a = 4.2251(6)$ Å, 27 nm crystallite size

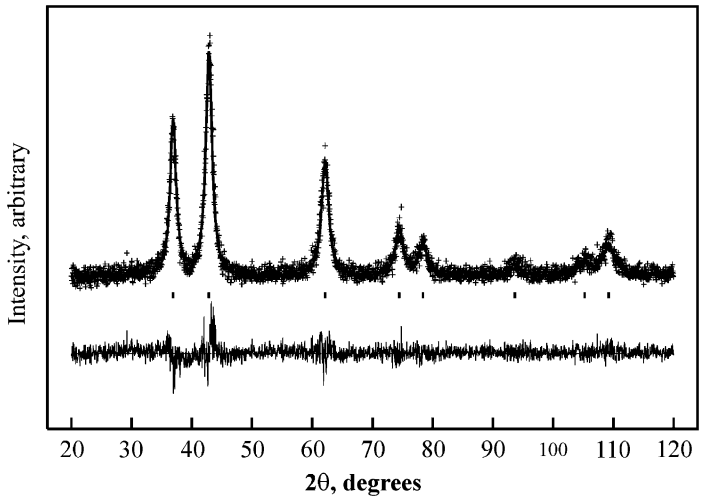

Fig. 3. Refined PXD pattern of sample annealed at 850 °C for 2 h, crosses mark the data points, upper solid line the profile fit and lower solid line the difference.

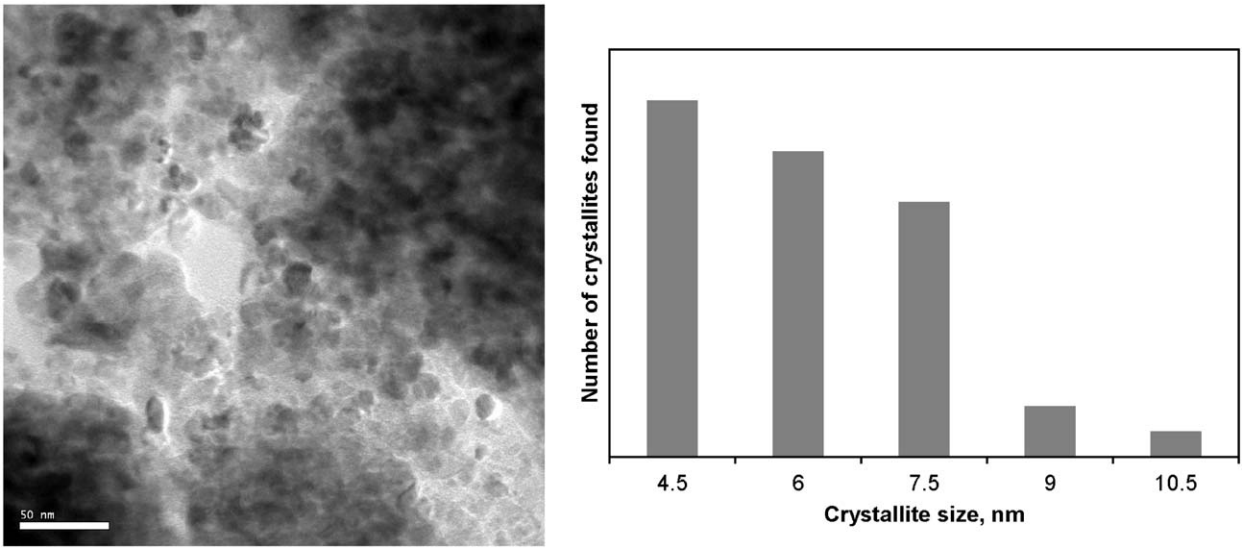

Fig. 4. Transmission electron micrograph and crystallite size distribution of $TiC_{0.18}N_{0.83}$ obtained by heating the precipitate at 1000 °C for 2 h.

from 450 to 1000 °C. However, all samples annealed in NH_3 atmosphere were nearly C-free (Table 1). These results are of interest for the creation of nanoparticle composites. Useful nanocomposite materials based on TiN require a crystallite size of less than 10 nm to attain maximum hardness [9]. Also, the introduction of C into TiN increases its hardness [19].

Annealing at 450 °C in N_2 yielded a solid that was X-ray amorphous. This corresponds to the material that was previously assigned to "amorphous Ti_3N_4" [7]. Chemical

analysis of the material produced here indicates that considerable carbon (and also some hydrogen) is present, with a bulk composition corresponding to $TiC_{0.22}N_{1.03}H_{0.07}$, or $Ti_3(C_{0.17}N_{0.78}H_{0.05})_{3.96}$ (Table 1). Assuming that C and N play similar structural roles within the material, the description of the material with a 3:4 ratio of cations to anions is justified. The black, X-ray amorphous solid was found to be electrically conducting. Infrared reflectance spectroscopy on a pressed sample of the powder showed a strong peak at 480 cm^{-1} with a shoulder extending up to ~800 cm^{-1}. The spectrum generally resembles that of rocksalt-structured Ti(C,N), produced by annealing at 1000 °C (Fig. 5). The IR active zone centre optic phonon (TO mode: Ti–N or Ti–C stretching vibrations) of well-crystallized stoichiometric TiN or TiC occurs near 500 cm^{-1}, and the *LO* modes extend up to ~800 cm^{-1} [20]. A feature at 2000 cm^{-1} in the spectrum of the $Ti_3(C,N,H)_4$ material corresponds to Ti–H stretching vibrations (Fig. 5). These are absent in the sample that has been annealed at 1000 °C.

TEM examination of the sample indicated the presence of nc material embedded in an amorphous matrix (Fig. 6). The nc particles gave face-centred cubic diffraction patterns with $a = 4.23$ Å, comparable with reported values for TiN_x and $Ti(C,N)_x$ [21] and were approximately 5 nm in dimension: however, these particles were all polycrystalline, so that the individual crystallite size was smaller than this. Lattice fringes of approximately 2.5 Å were observed for some particles. These could correspond to the 1 1 1 reflection of cubic rocksalt-structured TiN_x (2.47 Å [21]) or $Ti(C,N)_x$ nanoparticles. Electron diffraction patterns, Fig. 6, of the amorphous regions exhibited diffuse rings that occur at a similar *d*-spacing to the 2 0 0 and 2 2 0 reflections of crystalline TiN (i.e., the second and third rings of the crystalline pattern): that result could imply that short-range structural correlations present within the amorphous material are associated with an underlying rocksalt structure. EDX showed Ti, N and C (though samples were mounted on carbon grids) in nc and amorphous regions, suggesting that titanium nitride or carbonitride compositions are present throughout the sample.

Various $Ti(C,N)_x$ materials were examined by Raman spectroscopy. Normally, stoichiometric TiN or TiC with the rocksalt structure (i.e., *Fm*3*m* symmetry) have no first-order Raman-active vibrations. Well-crystallized samples close to the stoichiometric composition exhibit only weak second-order Raman scattering in experimental spectra [20]. However, the condition is relaxed if the samples contain defects or vacancies on cation/anion sites (Fig. 7). The spectra of materials prepared by annealing at 450 and 1000 °C, that correspond to X-ray amorphous $Ti_3(C,N)_4$ and nc Ti(C,N) compounds, respectively, are remarkably similar. Both generally resemble the spectrum obtained for highly defective TiN_x ($x = 0.59$) (Fig. 5) [20]. There is a broad band near 600 cm^{-1} that corresponds to combinations of acoustic and optic modes (Ti–N/Ti–C stretching vibrations), and a weaker feature at lower wavenumber (200–400 cm^{-1}) due to acoustic vibrations (Fig. 7). The Raman spectra generally indicate that both of the $Ti(C,N)_x$ materials prepared in this study have a similar local structure, that can be correlated with the underlying rocksalt structure of TiN or TiC, but large-scale disorder or defects.

3.2. X-ray absorption spectroscopy

XAS, along with analysis of the EXAFS, provides an ideal method for probing the local structure in disordered materials. Ti *K*-edge XAS data were obtained for samples annealed in N_2 atmosphere at temperatures from 400 to 1000 °C.

The absorption edge in the XAS occurs at ~4977.6 eV for samples annealed at 400–700 °C. This shifts to ca. 4979.2 eV for samples annealed between 900–1000 °C

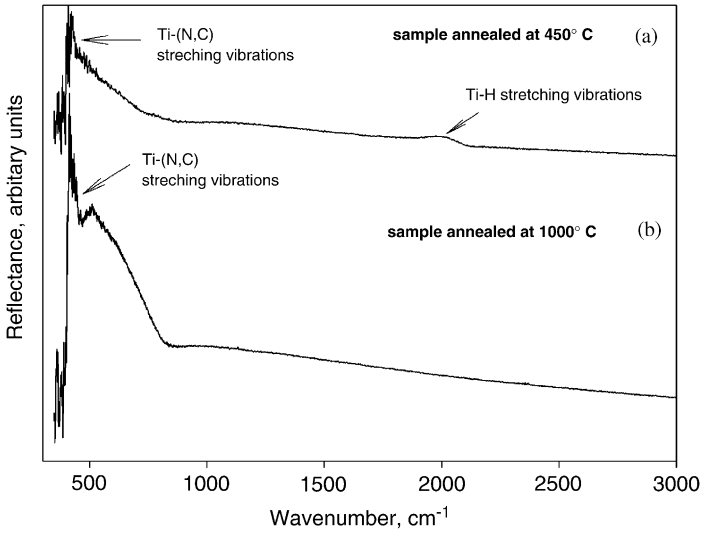

Fig. 5. Reflectance IR spectra of $Ti(C,N)_x$ materials annealed in N_2.

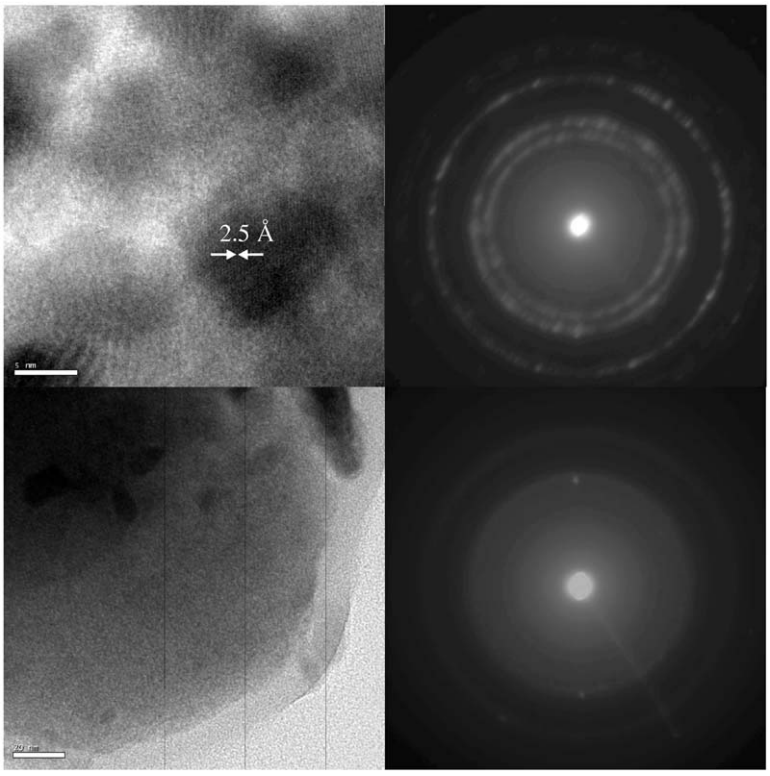

Fig. 6. Transmission electron micrographs (left) and electron diffraction patterns (right) of polycrystalline (top) and amorphous (bottom) regions of the material annealed at 450 °C.

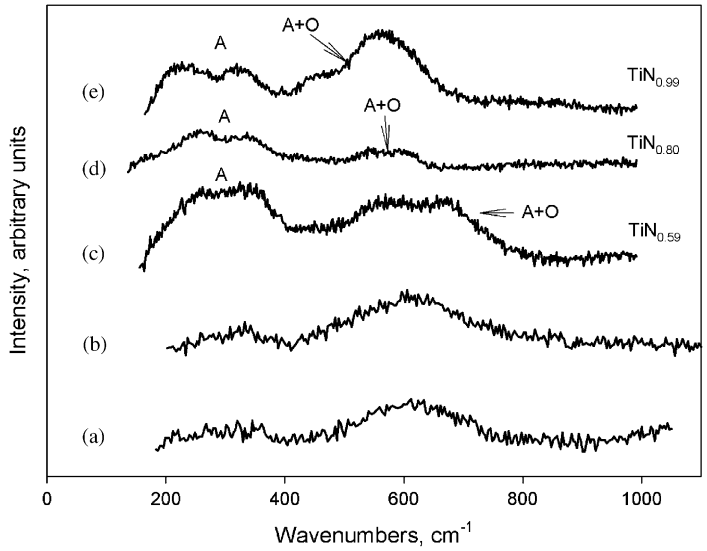

Fig. 7. Raman spectra of $Ti(C,N)_x$ materials annealed at (a) 450 °C or (b) 1000 °C and TiN_x materials with different compositions (c, d, and e). "A" represents acoustic branches; "A + O" represents combinations and overtones of acoustic and optic branches.

(Fig. 8). The change in the peak position occurs at the same temperature as the step change in the TGA plot, where the sample composition and degree of crystallinity is evolving rapidly. The edge position in the TiN standard was observed as 4978.0 eV.

The near-edge (XANES) region contains a strong (~14% of the intensity of the edge jump) pre-edge feature around 4968.4 eV for samples annealed at temperatures between 400 and 700 °C, which shifts to ~4970.8 eV after annealing at 800–1000 °C. The Ti pre-edge feature is associated with *s–d* electronic transitions that are not formally allowed for centrosymmetric sites. Such pre-edge features have been attributed to the presence of 4- or 5-coordinate Ti in titanium-bearing oxide systems, where it

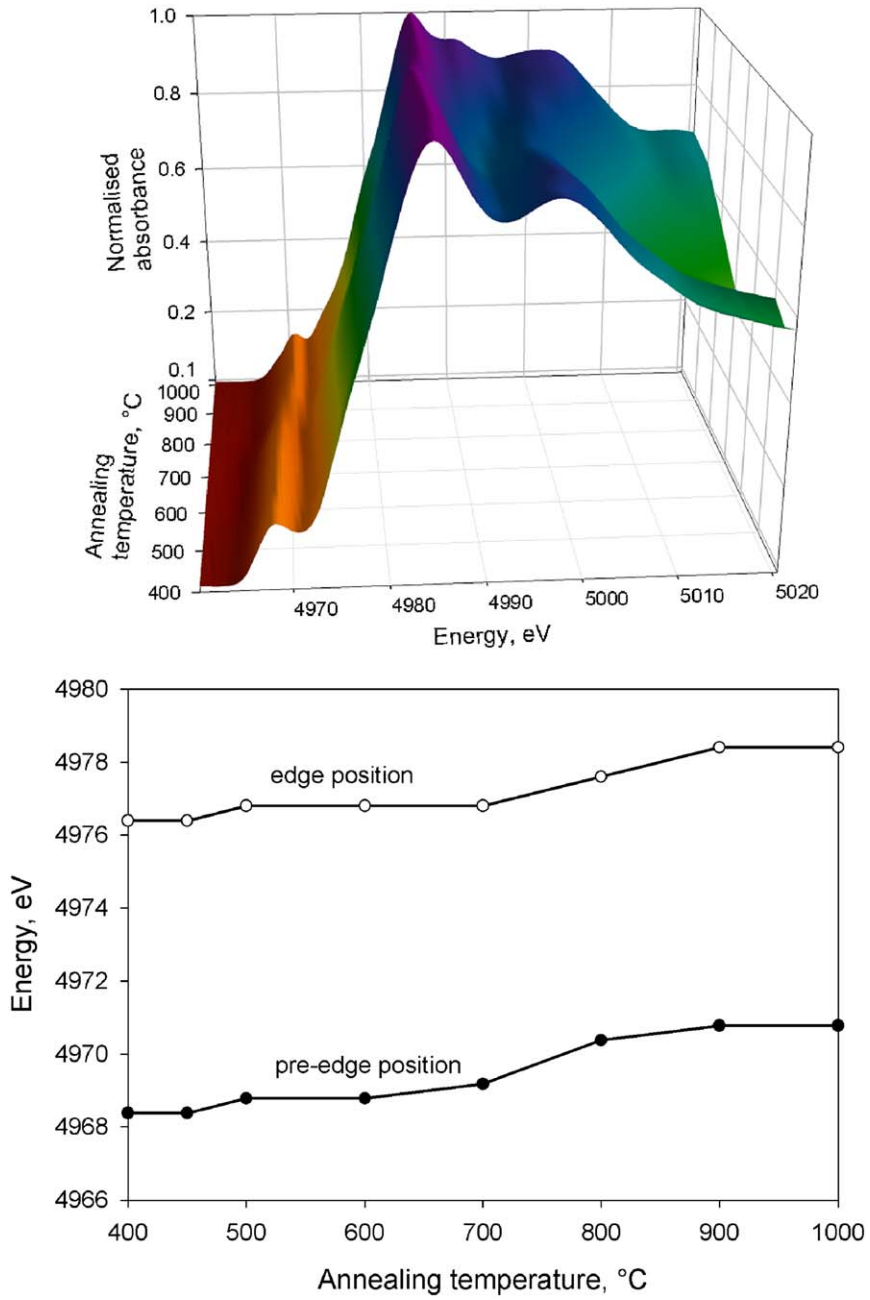

Fig. 8. Plots of the variation in the XAS spectra (top) and the Ti–K pre-edge and edge positions (bottom) with annealing temperature.

is known to be very weak or absent in materials that have 6-coordinated Ti^{4+} sites [22]. In rocksalt-structured TiN or TiC systems, normally no Ti *K*-pre-edge feature in XAS would be expected to appear, because all metal sites are centrosymmetric. However, the presence of vacancies within the structure, or (C,N) substitutions within the coordination sphere around the octahedral Ti sites, can destroy the centre of symmetry and result in relaxation of the selection rule. The pre-edge feature becomes slightly less intense as the annealing temperature is increased, but it remains clearly visible within the spectra in 1000 °C-annealed samples (Fig. 8). We recorded a similar intensity of the pre-edge feature within our TiN standard (~12%), that contained a small percentage of N vacancies (the analyzed composition was $TiN_{0.95}$: Table 1). The pre-edge peak position in the TiN standard was 4971.2 eV. We conclude that the pre-edge features observed in the spectra of samples annealed to high temperature (800–1000 °C) result from the presence of vacancies or (C,N) disorder on the anion sites in the rocksalt-structured crystalline materials. The pre-edge feature in the amorphous $Ti_3(C,N)_4$ samples obtained by annealing to within the 400–700 °C range could have a similar origin, or could be due to the presence of tetrahedrally coordinated $Ti(C,N)_4$

groups within that material. Ti_3N_4 is predicted to form a spinel structure that would contain TiN_4 as well as TiN_6 groups [4]. That possibility is examined below.

The Fourier-transformed Ti *K*-edge EXAFS data for all samples show two main peaks at ca. 2 and 3 Å (Fig. 9). These correspond to the first- and second-shell distances that are found within crystalline rocksalt-structured TiN or TiC. They occur at 2.12 and 3.00 Å for the TiN standard. The first distance corresponds to the Ti–N or Ti–C bond length with Ti in octahedral coordination within $Ti(C,N)_6$ groups, and the second represents Ti … Ti distances to the twelve surrounding Ti sites formed by edge centres within the face centred cubic cell. EXAFS oscillations from more distant shells were well resolved in our data for samples annealed at high temperature (800–1000 °C); as expected for the nc Ti(C,N) materials, these closely resemble the features for the TiN standard. Longer EXAFS correlations were not resolved in the data sets obtained for samples annealed at lower temperatures (400–700 °C), and these were not modelled in our study. If any tetrahedrally coordinated TiN_4 or TiC_4 groups were present in the samples annealed at low temperature, as would be expected from a spinel-structured model for the Ti_3N_4 composition, this would result in a Ti–N distance at ~1.9 Å. There is no evidence for any broadening of the first-shell peak for samples annealed at low temperature in our study that might indicate such short Ti–N components (Fig. 9). We conclude that the local structure of the amorphous $Ti_3(C,N)_4$ sample contains only sites with Ti–N(C) bond lengths that correspond to the octahedrally coordinated distances found in rocksalt-structured TiN or TiC.

The modelled bond lengths and first- and second-shell occupations for samples prepared within this study are listed in Table 2 and shown in Fig. 10 as a function of annealing temperature. The Ti–N distance remains around 2.04 Å for all samples annealed at 400–600 °C; it increases to 2.08 Å at 700 °C and above, whereas the Ti … Ti distance increases gradually from 2.96 Å at 400 °C to 3.00 Å between 700–1000 °C. These observations are all consistent with structural changes occurring within a rocksalt-structured framework of $Ti(C,N)_x$ materials. The second-shell Ti … Ti distance remains consistent with that expected for the B1 structure throughout the annealing series, although the occupation number increases abruptly

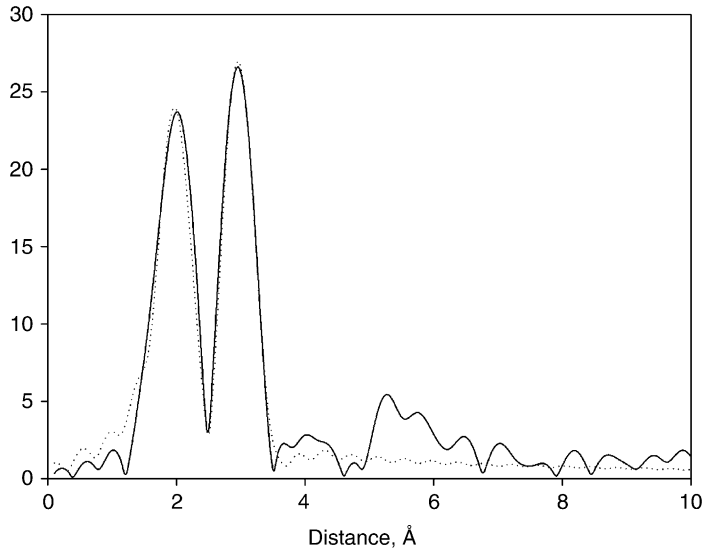

Fig. 9. Fourier transformed Ti *K*-edge EXAFS of the material annealed at 450 °C in N_2.

Table 2
Refined Ti *K*-edge EXAFS parameters obtained on samples annealed in N_2

Annealing temperature (°C)	R_1 (Ti–N) (Å)	σ^2	Coord. no.	R_2 (Ti … Ti) (Å)	σ^2	Coord. no.	*R* (%)
400	2.032(9)	0.022(1)	4.87(32)	2.962(7)	0.021(2)	4.48(32)	32.68
450	2.047(24)	0.022(5)	4.42(64)	2.971(8)	0.024(2)	4.51(36)	42.00
500	2.029(12)	0.028(3)	4.62(56)	2.987(10)	0.026(2)	5.58(54)	42.56
600	2.036(12)	0.028(5)	4.53(53)	2.994(13)	0.028(3)	5.67(57)	43.29
700	2.080(2)	0.020(6)	4.50(50)	3.000(1)	0.020(2)	5.00(49)	42.80
800	2.082(20)	0.020(1)	4.959(91)	3.008(11)	0.022(1)	10.95(102)	47.67
900	2.080(23)	0.010(6)	5.51(133)	2.995(13)	0.010(1)	9.96(117)	47.55
1000	2.100(20)	0.010(2)	6.07(129)	3.000(10)	0.010(1)	12.00(115)	51

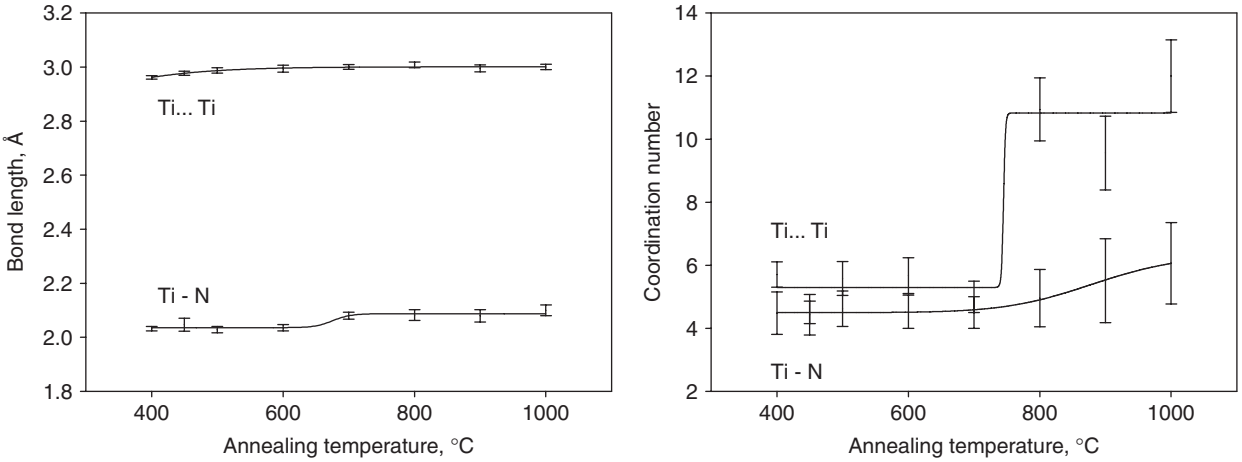

Fig. 10. Variation with annealing temperature of refined bond lengths and shell occupations from Ti *K*-edge EXAFS data.

at above 700 °C (Fig. 10). Below this temperature, the second-shell occupation is ~5.5, well below that expected for the rocksalt structure. This rises sharply to ~12 for samples annealed at high temperature, as expected for crystalline Ti(C,N) material containing few or no defects on the metal sites. The Ti–N shell has a determined coordination number of ~4.5 in samples annealed at temperatures up to 700 °C, this value then increases gradually with annealing until it achieves ~6 at the highest temperatures (Fig. 10).

3.3. Summary of the results and a structural model

The XAS results, along with the TEM and other studies, suggest the following structural model for the $Ti_x(C,N)_y$ materials prepared in this work. All of the solid-state materials obtained from the $Ti(NMe_2)_4/NH_3$ reaction precipitate by annealing at various temperatures have a local structure that is based on the rocksalt framework of TiN/TiC, including the amorphous part of the material annealed at 450 °C. Solid compounds obtained by annealing to below 700 °C have a high proportion (>50%) of vacancies on the Ti sites. The anion sites have a higher filling quotient (~75%, estimated from the first-shell occupation number determined from the EXAFS analysis). These sites are filled by N or C atoms derived from the precursor reaction, and perhaps also by H. This material constitutes X-ray amorphous "$Ti_3(C,N)_4$". Some regions within the samples achieve a degree of nanocrystallinity within the B1-structured motif that is detectable by electron diffraction/imaging (Fig. 6). It is unclear whether the same composition is present in both amorphous and nc regions, the amorphous parts may have higher carbon contents, but both are titanium nitride or carbonitride. Upon annealing to >700 °C, diffusion occurs at an appreciable rate and the structure begins to condense. Gaseous N- and C-bearing components are lost (the ratio of C/N removal depends upon the gas atmosphere during annealing), and the composition approaches the thermodynamically favoured stoichiometric TiN or Ti(C,N). The crystalline materials have nanoscale dimensions.

We propose that the amorphous solid formed by low-temperature annealing of the precursor is a highly defective, structurally disordered $Ti_x(C,N)_y$ material with the local arrangements of cations and anions based generally on the rocksalt structure type. Although the (C,N) vs. Ti ratio is increased over that of stoichiometric TiN or TiC, >50% of the second-shell Ti atoms are missing compared with the rocksalt structure: this causes the expected density to be less than half that of TiN or TiC. If useful properties such as the high hardness and toughness found for Ti(C,N) materials are maintained in this structure, it could provide a useful low-density alternative to Ti carbonitrides for various applications.

The low-density amorphous $Ti_3(C,N)_4$ material forms by condensation of oligomeric or polymeric units obtained from the ammonolysis of the $Ti(NMe_2)_4$ precursor. These units must be "pre-organized" to form a rocksalt structure due to their local coordination environments and the nature of the condensation reaction. Titanium(IV) amides often form oligomers [23] to obtain a higher coordination number, and the preferred symmetry is octahedral. This can be achieved here through bridging amides and the filling of vacant coordination sites by displaced amine molecules. Where a titanium centre is already attached to another titanium and undergoes ammonolysis, intramolecular condensation to form four-membered Ti_2N_2 rings should be facile and allows Ti to maintain octahedral geometry. Further, each substitution or condensation event will liberate one amine molecule and thus Ti can achieve coordinative saturation when only two imide bridges form, Fig. 11. The dimethylamine ligands can easily be lost, facilitating further ammonolysis and condensation, but the predisposition of this system to formation of a rocksalt-like lattice, even at low temperatures where diffusion is expected to be very limited, suggests that the formation of four-membered rings is dominant. The formation of "laddered" $[TaN]_5$ units was shown during ammonolysis of

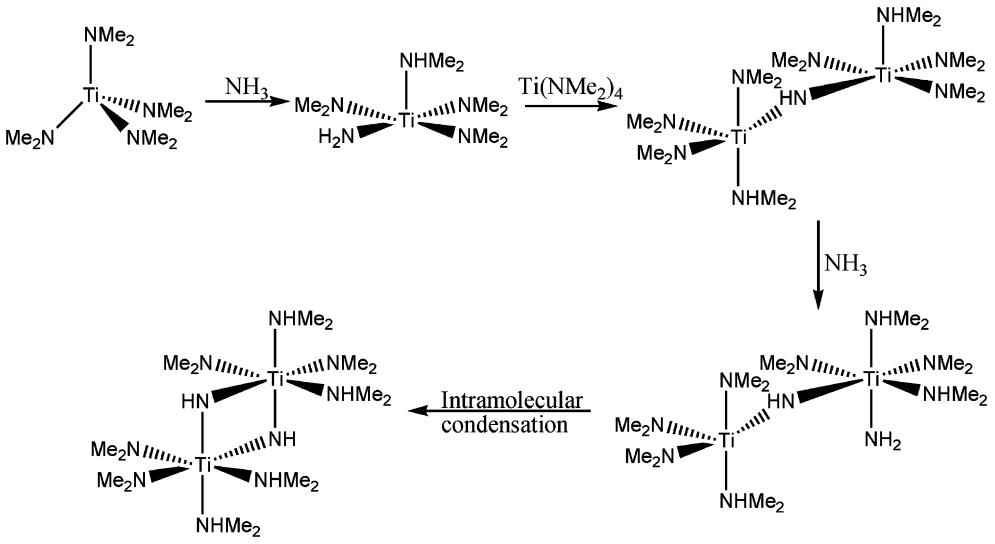

Fig. 11. Formation of Ti_2N_2 rings with saturated Ti-coordination sphere by intramolecular condensation.

(^{t}BuCH$_2$)$_3$Ta(CH^{t}Bu), where further ammonolysis followed by thermolysis produces cubic TaN [24]. In that case, flat-laddered structures were suggested to be formed due to the steric bulk of the ^{t}BuCH$_2$ groups. Here, octahedral symmetry can be maintained at the metal site even if the edge-linked Ti_2N_2 units are perpendicular to each other, since the fourth vertex of the square so formed can then be occupied by a bridging amine or amide ligand. Hence the outcome is likely to be significantly more complex than observed in the ammonolysis of (^{t}BuCH$_2$)$_3$Ta(CH^{t}Bu). However, a matrix formed in this way could clearly have an immobilized network in which the short-range structure resembles rocksalt. Large amounts of coordinated amine will still be present hence the initial polymeric material is rich in C-, N- and H-components ($TiC_{0.5}N_{1.1}H_{2.3}$). During initial heating (up to ~400 °C), terminal dialkylamide and amide groups are removed as amine and ammonia [7]. Some relaxation of the metal and anionic sublattices is likely to occur, although large-scale diffusion and bond rearrangement do not occur below ~700 °C. The composition approaches that of $Ti_3(C,N)_4$, in which the Ti atoms within nanosized regions are placed on the positions of the rocksalt lattice, with ~50% occupancy, and (C,N) atoms occupy the anion sites (with slightly greater occupancy). When one considers the disorder which would result from condensation of cages formed through a process like that described above, it is unsurprising that the structure is so defective. Finally, during heating to ~700 °C, bond reformation and local diffusion processes become significant, and the structure rearranges and condenses into the thermodynamically stable TiN or Ti(C,N) phase, in equilibrium with the N_2 or NH_3 gas atmosphere.

4. Conclusions

We investigated the solution phase reaction between tetrakisdimethylamidotitanium ($Ti(NMe_2)_4$) and ammonia that precipitates $TiC_{0.5}N_{1.1}H_2$ [3]. These are useful precursors to TiN or Ti(C,N) materials. The decomposition reaction proceeds in two steps to yield rocksalt-structured material. Heating to ~700 °C in NH_3 yields TiN; however, heating in N_2 leads to $TiC_{0.2}N_{0.8}$. The materials form nanoparticles, with sizes in the 4–12 nm range. Heating to between the two steps in the TGA curve (~450 °C) gives rise to a material that is X-ray amorphous, with bulk composition $Ti_3(C_{0.17}N_{0.78}H_{0.05})_{3.96}$. TEM studies indicate that the material contains nanocrystals (<5 nm) embedded in an amorphous matrix. The local structure of the X-ray amorphous solid is related to the rocksalt Ti(C,N) phase, but with a large proportion of vacancies on both the cation (Ti) and anion (C,N) sites. The first shell Ti coordination is approximately 4.5 and the second-shell coordination is 5.5, compared with values of 6 and 12, respectively, expected for the rocksalt structure. The amorphous material is ~50% less dense than Ti(C,N). The structure is suggested to result from the condensation of Ti_2N_4 species formed during ammonolysis of $Ti(NMe_2)_4$. These materials could provide useful precursors for synthesis of ultra-hard nanocomposites within the Ti–N–C system.

Acknowledgments

ALH is supported through a Royal Society University Research Fellowship. PFM is supported by the EPSRC (Grants GR/R65206 and GR/S78704) and also receives support through a Wolfson Foundation—Royal Society Research Merit Award/Fellowship. This work here was funded by EPSRC under Grants GR/S10155/01 (AWJ) and GR/R65206/01 (OS). The authors thank CCLRC for beamtime at the SRS (Award 43057), Dr F. J. W. Mosselmans for assistance with the XAS data collection, and Drs. B. A. Cressey (University of Southampton) and

S. Firth (UCL) for collecting TEM data, as well as Epichem for a gift of the $Ti(NMe_2)_4$ starting material.

Appendix A. Supplementary materials

Supplementary data associated with this article can be found in the online version at doi:10.1016/j.jssc.2006.01.067.

References

[1] H.C. Chen, B.H. Tseng, M.P. Houng, W.H. Wang, Thin Solid Films 445 (2003) 112;
C. Mitterer, P.H. Mayrhofer, Key Eng. Mater. 264–268 (2004) 453;
D.J. Blackwood, J. Corros. Rev. 21 (2003) 97;
G.B. Smith, A. Ben-David, P.D. Swift, Renew. Energy 22 (2001) 79.
[2] R.M. Fix, R.G. Gordon, D.M. Hoffman, Chem. Mater. 3 (1991) 1138;
B.H. Weiller, S.D. Adamson, J. Electrochem. Soc. 144 (1997) L40;
B.H. Weiler, J. Am. Chem. Soc. 118 (1996) 4975.
[3] L.H. Dubois, Polyhedron 13 (1994) 1329.
[4] W.I. Ching, S.-D. Mo, L. Ouyang, I. Tanaka, M. Yoshiya, Phys. Rev. B 61 (2000) 10609.
[5] A. Zerr, G. Miehe, G. Serghiou, M. Schwarz, E. Kroke, R. Riedel, H. Fueß, P. Kroll, R. Boehler, Nature 400 (1999) 340;
K. Leinenweber, M. O'Keefe, M. Somayazulu, H. Hubert, P.F. McMillan, G.W. Wolf, Chem. Eur. J. 5 (1999) 3076.
[6] A. Zerr, G. Miehe, R. Riedel, Nat. Mater. 2 (2003) 185.
[7] D.V. Baxter, M.H. Chisholm, G.J. Gama, V.F. DiStasi, A.L. Hector, I.P. Parkin, Chem. Mater. 8 (1996) 1222.
[8] G.M. Brown, L. Maya, J. Am. Ceram. Soc. 71 (1988) 78.
[9] J. Patscheider, MRS Bull. (2003) 180.
[10] L. Zhu, M. Ohashi, S. Yamanaka, Mater. Res. Bull. 37 (2002) 475.
[11] S. Kaskel, K. Schlichte, G. Chaplais, M.J. Khanna, J. Mater. Chem. 13 (2003) 1496.
[12] A.L. Hector, I.P. Parkin, Chem. Mater. 7 (1995) 1728;
R.A. Janes, M. Aldissi, R.B. Kaner, Chem. Mater. 15 (2003) 4431.
[13] R. B. Von Dreele, A. C. Larson, Generalized structure analysis system, Los Alamos National Laboratory, NM87545, USA (December 2002 release).
[14] E. Soignard, P.F. McMillan, Chem. Mater. 16 (2004) 3533.
[15] N. Binsted, Program for the analysis of X-ray absorption spectra, version 3.33, University of Southampton, UK, 1998.
[16] N. Binsted, Excurve 9.271, University of Southampton, UK, 2003.
[17] A.L. Hector, A.W. Jackson, P.F. McMillan, O. Shebanova, Mater. Res. Soc. Symp. Proc. 848 (2005) FF2.3.1.
[18] L. Loffelholz, J. Engering, M. Jansen, Z. Anorg. Allg. Chem. 626 (2000) 963.
[19] H.J. Holleck, Vac. Sci. Technol. A 4 (1986) 2661.
[20] W. Spengler, R. Kaiser, A.N. Christensen, G. Müller-Vogt, Phys. Rev. B 17 (1978) 1095.
[21] Powder Diffraction File, version 2.4, International Center for Diffraction Data, Swarthmore, PA 19073, USA, 2004.
[22] G.E. Brown Jr., G. Calas, G.A. Waychunas, J. Petiau, Rev. Miner. Geochem. 18 (1988) 431.
[23] D.C. Bradley, M.H. Gitlitz, J. Chem. Soc. A (1969) 980.
[24] M.M. Banaszak Holl, P.T. Wolczanski, G.D. Van Duyne, J. Am. Chem. Soc. 112 (1990) 7989.